

QuEMAT: Query-based Explainable Multi-annotator Tendency Learning

Liyun Zhang
Osaka University
Japan

liyun.zhang@lab.ime.cmc.osaka-u.ac.jp

ABSTRACT

Multi-annotator tendency learning aims to model the specific behavior patterns of each annotator. However, existing methods mainly focus on the tendencies of individual annotators, overlooking the correlations between different annotators, leading to inadequate modeling of the label distribution of the original dataset. Additionally, current methods cannot visualize the decision-making process of each annotator, resulting in a “black-box” output. Therefore, we propose an explainable multi-annotator tendency learning framework, QuEMAT. Specifically, we preserve both individual annotator tendencies and the correlations between different annotators, maximizing the retention of label distribution in the original dataset. Meanwhile, we visualize each annotator’s tendency, providing interpretable insights into the behavior of each annotator. Moreover, the sparse per-annotator labels in existing datasets hinder the advancement of this area. To this end, we additionally construct two large-scale datasets: AMRE and STREET. It is worth noting that AMRE is the first multi-annotator multimodal dataset in this field. Extensive experiments show that our model is more effective than the latest methods.

CCS CONCEPTS

• Computing methodologies → Multi-task learning.

KEYWORDS

Multi-annotator learning, Annotator tendency, Multi-annotator datasets, Explainable Multi-annotation

1 INTRODUCTION

Reliable annotations of training samples are crucial in machine learning. *Reliable* here means that the same concept is always annotated with the same label. However, in real-world scenarios, different annotators often provide distinct interpretations of the same sample [26, 32]. This multi-annotator scenario is particularly common in fields such as medical image analysis [19], sentiment analysis [17], and visual perception [42], where subjective judgment and varying levels of expertise lead to significant differences between annotators, thereby hindering label consistency.

Permission to make digital or hard copies of all or part of this work for personal or classroom use is granted without fee provided that copies are not made or distributed for profit or commercial advantage and that copies bear this notice and the full citation on the first page. Copyrights for components of this work owned by others than the author(s) must be honored. Abstracting with credit is permitted. To copy otherwise, or republish, to post on servers or to redistribute to lists, requires prior specific permission and/or a fee. Request permissions from permissions@acm.org.

© 2025 Copyright held by the owner/author(s). Publication rights licensed to ACM.
ACM ISBN 978-x-xxxx-xxxx-x/YY/MM
<https://doi.org/10.1145/nnnnnnn.nnnnnnn>

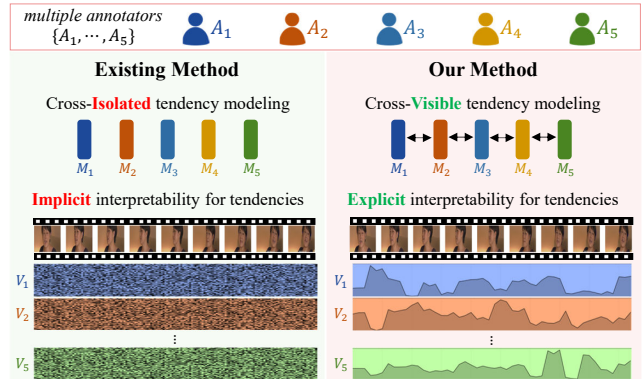


Figure 1: Method comparison. In this figure, we take five annotators $A_i, i \in \{1, \dots, 5\}$ as an example. We use M_i and V_i to represent the model and visualization results for annotator A_i , respectively. Existing methods overlook the correlations of the inter-annotator tendencies and fail to explain the behavior patterns of each annotator. In contrast, our method addresses these issues.

To learn more reliable models in multi-annotator scenarios, researchers introduce a task called *multi-annotator learning*. Multi-annotator tendency learning aims to model the specific behavior patterns of each annotator to capture their individual preferences and provide interpretability. In contrast, multi-annotator learning mainly utilizes extracted annotator features for specific tasks, emphasizing task objectives without explaining individual annotator factors. Most multi-annotator learning approaches are typically dedicated to simultaneously learning different characteristics (e.g., confusion mode [34], agreement [37], expertise level [12]) from multiple annotators, then applying them to specific tasks, e.g., classification, segmentation, or multi-annotator aggregation, through majority voting or probabilistic aggregation. While these methods have shown success in certain applications, they often treat annotator discrepancies as noise rather than valuable information [14, 40]. Existing research on multi-annotator tendency learning is currently sparse, some recent works similar to it have attempted to model individual annotator behaviors through various techniques such as confusion matrices [11] or neural networks with annotator-specific parameters [9] to understand more about individual annotator tendencies, thereby helping to better implement specific tasks.

However, as shown in Figure 1, current multi-annotator tendency learning methods have several issues. First, existing methods focus merely on the trends of individual annotators. For example,

they build independent models [10], distributions [19], or confusion matrices [42] for each annotator to capture annotator-specific tendencies. These methods overlook the correlations between annotators, leading to inadequate modeling of the label distribution in the original dataset. Second, existing models [4] lack clear interpretability, or they only implicitly reveal trends where certain annotators play a larger role in the labeling process [6].

To address these challenges, we propose QuEMAT, an attention-based multi-annotator model. Firstly, it leverages learnable queries in the Q-Former (query transformer) [16] to model specific annotators, using a cross-attention module to interact with input features and capture individual tendency patterns of the intra-annotator. Simultaneously, all queries can interact as a whole in a self-attention module, making them visible to each other to learn the correlations of the inter-annotator tendencies. This avoids the limitations of only learning intra-annotator tendency patterns in isolation and enhances the interpretability of inter-annotator correlations, while also reducing the cost of building separate models for each annotator. Secondly, benefiting from the attention architecture of Q-Former, cross-attention interactions between annotator-specific queries and input features capture each annotator’s tendency to focus on the input information. This interaction is explicitly visualized through attention weights, clearly indicating which parts and to what extent differences in the input information are emphasized by each annotator’s tendency. This greatly improves the interpretability of each annotator’s pattern and enhances the transparency of the model.

However, even with efficient modeling methods, multi-annotator tendency learning still faces the challenge of data sparsity in practical applications [22]. Although crowdsourcing platforms have numerous annotators for annotating, only a very small subset of samples are provided consecutive annotations with consistent IDs. This sparsity in consecutive annotator labels poses a significant challenge for learning reliable annotator-specific tendencies. To this end, we constructed two large-scale datasets: STREET (city impression evaluation) and AMER (video emotion recognition), each providing substantial consecutive labels per annotator ID, respectively, offering valuable open-source resources to the community. It is worth noting that AMRE is the first multi-annotator multimodal dataset in this field. Our work makes the following key contributions:

- **A novel multi-annotator tendency learning framework:** We propose an attention-based model that uses learnable queries to model individual annotators while learning inter-annotator correlations, providing explicit interpretability through visualization of attention weights to make it possible to understand whether the model has effectively learned the tendencies of individual annotators.
- **An insight about multi-annotator tendency learning:** After research, we found that through modeling the behavior patterns of individual annotators, we can gain more information about the annotator’s tendency, thereby helping to better implement specific tasks.
- **Two large-scale datasets with dense per-annotator labels:** We contribute two new datasets: STREET (city impression evaluation) and AMER (video emotion recognition),

providing averages of 4,300 and 3,118 annotations per annotator respectively, alleviating the sparse per-annotator labels challenge in multi-annotator tendency learning research.

2 RELATED WORK

2.1 Multi-annotator Tendency Learning Task

To the best of our knowledge, the multi-annotator tendency learning task problem has not yet been investigated. Traditional multi-annotator learning tasks focus on estimating true labels from multiple noisy annotations. Such as early probabilistic models [8], EM algorithms [39], Gaussian models [30], and biased estimation [38]. Tanno et al. [35] proposed modeling annotator confusion matrices as learnable parameters in neural networks. Cao et al. [3] introduced max-MIG to learn from multiple annotators. NEAL [5] employs neural expectation-maximization to jointly learn annotator expertise and true labels. Later methods used probabilistic frameworks to aggregate multiple annotations into a ground truth label by confusion matrix [34], agreement distribution [37], and Gaussian distributions [19]. These methods often treat individual annotator discrepancy as noise rather than valuable information [14, 40]. In contrast, multi-annotator tendency learning by our defined aims to model each annotator to capture specific behavioral patterns and providing interpretability. Some recent works similar to it have attempted to model individual annotator behaviors through confusion matrices [11] or annotator-specific network parameters [9] to understand more about individual annotator tendencies, thereby helping to better implement specific tasks. However, these approaches lack interpretability.

2.2 Multi-annotator Datasets

Learning reliable annotator-specific tendencies typically requires sufficient consecutive individual annotator labels. However, most existing multi-annotator datasets suffer from sparsity labels, with each annotator typically labeling only a small portion of the data. CIFAR-10H [23], based on the CIFAR-10 [15] dataset, includes 10,000 test samples labeled by 2,571 annotators, but each annotator ID has on average only about 200 consecutive labels. LabelMe [27] includes an average of approximately 42.4 consecutive labels per annotator ID. Audio dataset Music [29] contains an average of about 46.1 consecutive labels. The medical datasets are commonly used in multi-annotator studies, consecutive annotator labels are even sparser. QUBIQ [13], a dataset for quantifying uncertainty in biomedical image segmentation, includes four distinct segmentation datasets with an average of only 40 samples, and even then, annotator IDs have only around 8 consecutive labeled samples each. This sparsity poses a significant challenge for the multi-annotator tendency learning task. To this end, we contribute two large-scale datasets: STREET and AMER, averaging 4,300 and 3,117.8 consecutive labels per annotator ID, respectively. These datasets contribute significant open-source resources that we believe will benefit the research community.

2.3 Annotator Tendency Learning Framework

Previous studies typically construct independent models for each annotator to learn their specific behavioral patterns [10], or build

Table 1: Dataset comparison. Compared to existing multi-annotator datasets, our dataset contains a greater number of samples annotated by each annotator, which helps promote annotator tendency learning. Meanwhile, AMER is the first multimodal multi-annotator dataset.

| Dataset | Dataset description | Modality | # samples per annotator |
|----------------------|-----------------------------------|--------------------|-------------------------|
| QUBIQ-kidney [20] | kidney image | image | 24 |
| QUBIQ-tumor [20] | brain tumor image | image | 32 |
| QUBIQ-growth [20] | brain growth image | image | 39 |
| QUBIQ-prostate [20] | prostate image | image | 55 |
| CIFAR-10H [24] | object recognition | image | 200 |
| MUSIC [28] | music genre classification | audio | 2~368 |
| MURA [25] | radiographic image | image | 556 |
| RIGA [1] | retinal cup and disc segmentation | image | 750 |
| LIDC-IDRI [2] | lung nodule image | image | 1,018 |
| STREET (Ours) | city impression evaluation | image | 4,300 |
| AMER (Ours) | video emotion recognition | audio, video, text | 970~5,202 |

separate distributions based on input features to fit each annotator [19], or use individual confusion matrices to approximate each annotator’s tendencies [42]. These independent models lead to increased computational costs, and completely isolated modeling of annotators’ tendencies is not beneficial for interpreting relationships among annotators’ tendencies. Meanwhile, recent research typically only provided implicit interpretability for annotator tendencies, mainly by associating annotator influences with model outcomes. For instance, TAX [6] explains pixel-level assignment decisions for semantic segmentation by associating learned convolutional kernels with a prototype library representing annotator tendencies. MAGI [43] leverages multiple annotators’ explanations addressing challenges of noisy annotations and missing annotator correspondences. Schaeckermann et al. [31] revealed how factors like expert background and data quality contribute to annotation disagreements. However, this makes it difficult to explicitly show which specific elements in the scene each annotator, based on their tendencies, focuses on. To mitigate these issues, we proposed an efficient and interpretable framework for multi-annotator tendency learning. We use learnable queries to model both intra-annotator patterns and inter-annotator correlations, avoiding isolated modeling of each annotator while providing explicit interpretability of the discrepancy in annotator tendencies.

3 DATASET CONSTRUCTION

This paper focuses primarily on annotator tendency learning. For this task, the most important factor is the number of samples annotated by each annotator. Table 1 compares the current multi-annotator datasets. We observe that in existing datasets, the number of samples annotated by each annotator is relatively limited, and there is a lack of multi-annotator multimodal datasets. For example, in the RIGA dataset [1], each annotator labels 750 samples; while in the CIFAR-10H dataset [24], each annotator labels 200 samples. These datasets are insufficient for annotator tendency learning. To fill this gap, we introduce two new datasets: the city impression assessment dataset STREET and the multi-modal emotion recognition dataset AMER. These datasets provide enough single-annotator annotations to meet the requirements of annotator tendency learning.

(1) **STREET** is an urban perception dataset with multi-annotators, which contains 4,300 high-resolution images covering various urban elements, such as streets, public spaces, and infrastructure. The images and labels come from a study to capture emotions associated with cities.¹ Each image is annotated by 10 annotators, assessing five perception dimensions: happiness, healthiness, safety, liveliness, and orderliness, using a 7-point scale (−3 to +3). This multi-annotator dataset provides comprehensive human perception data for urban environments, enabling the quantitative analysis of environmental features and their emotional impact.

(2) **AMER** is a multimodal emotion dataset, which contains 5,207 video samples. This dataset is derived from MER2024 [18], which offers multi-annotator emotion labels. The AMER dataset consists of 13 annotators, where each annotator selects the most likely label from 8 candidate labels, i.e., worry, happiness, neutrality, anger, surprise, sadness, other, and unknown. Among all annotators, 10 annotators show consistent participation, each providing approximately 970 to 1,096 labels, while the remaining 3 annotators contribute over 5,000 labels each. This rich multi-annotator setup provides reliable emotion annotation results and allows for a robust evaluation of emotion recognition performance.

4 METHODOLOGY

4.1 Overview

QuEMAT mainly consists of two key parts: query-based specific annotator modeling and attention-based interpretable tendencies. Based on the classification task, they are achieved by a pre-trained image encoder, the annotator-specific learnable queries representing the tendencies of multi-annotators, a frame and video Q-Former, and the classifiers for corresponding annotators, as shown in Figure 2.

Note that this architecture is specifically designed for video inputs from the AMER dataset. For experiments on the STREET image dataset, we replace the frame and video Q-Former modules with a single image Q-Former architecture, which is detailed in the supplementary material. Also, all experiments involving the

¹We are currently negotiating to publish the dataset.

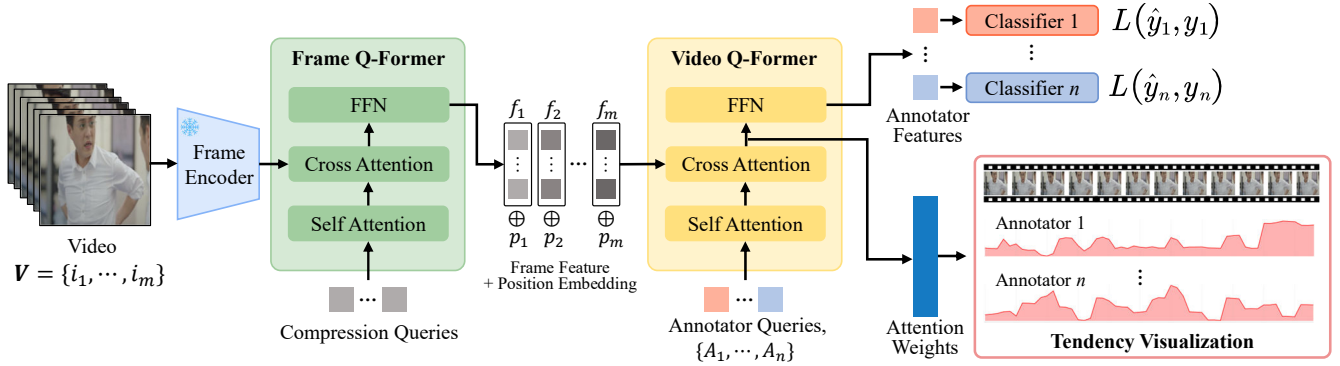


Figure 2: Illustration of our QuEMAT architecture. A frozen pre-trained encoder extracts frame features, which are compressed through the Frame Q-Former. With added frame position embedding, these interact with $1, \dots, n$ annotator-specific learnable queries in the Video Q-Former through cross-attention, producing annotator-specific features for classification. Each annotator’s cross-attention weights from Video Q-Former represent annotator tendencies and are visualized for interoperability.

STREET image dataset consistently employ this image-specific architecture as described in the supplementary material.

4.2 Query-based Specific Annotator Modeling

We proposed a query-based specific annotator modeling approach inspired by Q-Former [16]. As Fig. 2 illustrates, given a video input $V \in \mathbb{R}^{T \times H \times W \times 3}$, a frozen pre-trained image encoder [33] first extracts frame features, which are then further compressed by the image Q-Former using a specific number of compression queries, typically 32, to alleviate subsequent computational costs [16]. The frame position embedding is then added and input to the video Q-Former. Subsequently, we define the unique tendency pattern for annotator A_k ($k = 1, \dots, n$) through each learnable query in a Q-Former, then all annotator-specific queries in cross-attention simultaneously interact with input features to capture their diverse tendencies and obtain annotator-specific feature. Finally, the specific annotator features are mapped through a fully connected layer to an appropriate feature dimension and then connected to each annotator’s corresponding classifier to output classification results. Note that although we assign a separate query for each annotator, they are processed by a multi-head attention module, typically with 12 heads. This setup provides each query with diverse perspectives. Our experiments have verified that the learned tendency information is as expected and effective.

This design not only significantly alleviates the overhead of building a separate model for each annotator but also avoids learning each annotator’s pattern in isolation while ignoring the inter-annotator’s correlations. That is, the attention mechanism based on Q-Former enables each independent annotator query to learn relationships between annotators in a self-attention module, then while interacting with input features through cross-attention to capture individual tendencies. This significantly improves over the limitations of current methods, achieving efficient modeling for each annotator while enhancing the interpretability of annotators’ tendency relationships.

4.3 Attention-based Interpretable Tendency

Our method benefits from the attention architecture of Q-Former. By defining each annotator’s specific tendency pattern with learnable queries, our approach leverages cross-attention interactions between annotator-specific queries and input features, capturing each annotator’s distinct focus on the input information, output in the form of attention weights. This attention weight enables clear and explicit visualization of the different parts and degrees of input information that each annotator focuses on based on their tendencies, greatly enhancing the ability to verify whether the model has effectively learned each annotator’s pattern and improving the transparency of the overall model. As shown in Figure 2, the attention to video input is based on all frames of the video. Different annotators’ varying levels of attention to different frames indicate their tendency differences. The comparison curves more intuitively illustrate these differences: annotator 1 shows more attention to the final frames, while annotator n focuses more on the middle frames. This task is video emotion classification. Considering the annotation results and observing the video sample, we see that both annotators labeled emotions like anger and worry. The frames they focus on correspond to segments in the video that also align with these expected emotions.

4.4 Loss Function

Finally, as shown in Figure 2, the total training loss $\mathcal{L}_{\text{total}}$ for the proposed multi-annotator classification model, QuEMAT, is defined as the sum of individual cross-entropy losses for each annotator:

$$\mathcal{L}_{\text{total}} = \sum_{k=1}^n \mathcal{L}(\hat{y}_k, y_k), \quad (1)$$

where each annotator A_k has a specific predicted probabilities $\hat{y}_k \in [0, 1]^C$, a reference label $y_k \in \{0, 1\}^C$ in one-hot vector representation, and C is the number of classes.

5 EXPERIMENT

We conduct extensive experiments to evaluate our QuEMAT with competing approaches, primarily focusing on individual annotator modeling, inter-annotator consistency distributions, and demonstrating our advantages in providing explicit interpretability of annotator tendencies. To verify the effectiveness of QuEMAT, we introduce three representative baselines: D-LEMA [21] is an ensemble architecture for multi-annotator learning; PADL [19] uses Gaussian distribution fitting each annotator’s tendency pattern; MaDL [11] employs individual confusion matrices to approximate each annotator’s tendency. Meanwhile, to verify that the model has truly learned the tendency information rather than the features from the encoder, we specifically set a Base baseline that only retains the encoder and classifiers as a reference. We evaluate and discuss results on two novel datasets we introduced with relatively large-scale per-annotator labels. Note that additional experiments are provided in the supplementary material such as additional results and model efficiency, etc.

5.1 Implementation Details

For the model pipeline (see Figure 2), we use ViT-G/14 from EVA-CLIP [33] as the encoder, with the image Q-Former initialized from InstructBLIP [7] and the video Q-Former initialized from VideoLLaMA [41]. The input image/video is resized to 224×224 and further normalized. The number of query tokens matches the number of annotators, and each annotator’s classifier model uses an MLP. During training, we use the AdamW optimizer with an initial learning rate of 1e-4, weight decay of 0.01, and a maximum gradient norm of 1.0 for gradient clipping. A linear warmup strategy is applied for the first 20% steps followed by cosine learning rate decay. We set the maximum number of epochs to 200, with early stopping (patience being 25) to prevent overfitting. To accelerate training, the model is trained using distributed data parallel (DDP) on four NVIDIA V100 GPUs.

5.2 Evaluation Metrics

For evaluating multi-annotator tendency learning, accuracy is the fundamental metric. To show the model’s capability to capture annotators’ tendencies, we propose a new metric, coined difference of inter-annotator consistency.

Difference of inter-annotator consistency (DIC) is utilized to measure how well a model preserves the inherent disagreement patterns among annotators. The annotations given by different annotators differ, and their consistency can be measured by Cohen’s kappa coefficient [36]. Let Y_k and Y_l denote the set of all annotations by annotators A_k and A_l . We can compute *inter-annotator consistency matrix* M whose (k, l) -th element m_{kl} is given by

$$m_{kl} = \kappa(Y_k, Y_l), \tag{2}$$

where $\kappa(Y_k, Y_l)$ gives Cohen’s kappa coefficient for Y_k and Y_l . We can also compute the inter-annotator consistency matrix M' but for predictions \hat{Y}_k and \hat{Y}_l , where its (k, l) -th element m'_{kl} is given by

$$m'_{kl} = \kappa(\hat{Y}_k, \hat{Y}_l). \tag{3}$$

Ideally, these matrices should be the same, but due the model’s bias can cause discrepancy between them. We quantify such differences in inter-annotator consistency by

$$\text{DIC} = \|M - M'\|_F, \tag{4}$$

where $\|\cdot\|_F$ denotes the Frobenius norm. A lower DIC indicates that the model successfully captures each annotator’s tendency (with respect to the others).

5.3 Quantitative Results

For individual annotator modeling, the accuracy scores in Tables 2 and 3 demonstrate that our method achieves higher scores on both datasets: STREET (covering five perception dimensions: happiness, healthiness, safety, liveliness, and orderliness) and AMER for each annotator. Particularly, our method consistently outperforms other models in terms of average accuracy. In addition, by comparing the results with the Base baseline, it can be proved that the model learned effective annotator information. For inter-annotator consistency, the DIC scores in Table 4 also show that our method surpasses baseline approaches on both STREET and AMER datasets. We indirectly quantify each annotator’s specific tendency through the inter-annotator consistency matrices. These comparative results verify the superiority of our proposed method in modeling individual annotators and inter-annotator consistency distributions.

5.4 Qualitative Results

We qualitatively examine the interpretability of annotator tendencies by visualizing the attention weights over frame features² with respect to each annotator’s query in the cross-attention mechanism in Q-formers.

As shown in Figure 3, on the AMER dataset, annotators demonstrate diverse preferences through their varying attention to different frames. The comparison curves illustrate these differences more intuitively: Annotator 1 shows higher attention to the final frames (45-50), while Annotator 13 focuses more on the early frames (5-10), the same as Annotator 4. Annotator 10 shows a different focus. For this video emotion classification task, Annotator 1 predicted “sad”, while Annotator 4 and 13 predicted “worried”. Analysis of the original video and Ground Truth labels. Annotators’ focus meets the expectations. The frames highlighted by our model’s learned annotator tendencies correspond to consistent emotional cues in the video, validating both the effectiveness of our model and its superior interpretability.

As illustrated in Figure 4, on the STREET dataset, annotators exhibit different tendencies through their varying attention to distinct semantic elements within the same input image. The highlighted attention regions reveal these differences: Annotators 3, and 7 centralized focus more on the sculpture in the image, while other annotators show less attention to this element. This task involves impression evaluation across five dimensions (happiness, healthiness, safety, liveliness, and orderliness) on a scale from -3 to +3. Analyzing the original image content and prediction results reveals that Annotators 3 and 7 gave high ratings on happiness and healthiness dimensions, which aligns with the peaceful and

²For the STREET dataset, the attention weights over patch features.

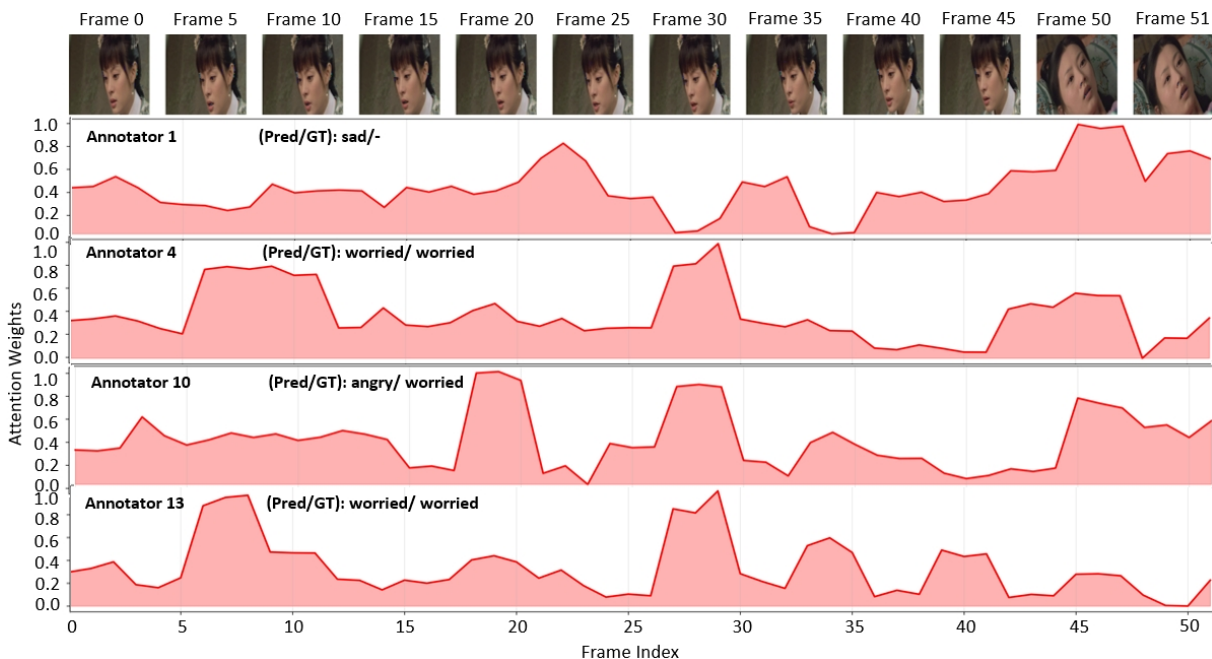


Figure 3: We visualize the interpretable annotator tendencies on the AMER dataset. The attention patterns of multi-annotators reveal distinct preferences, where annotator 1 exhibits notably high attention to final frames (containing different characters) compared to annotators 4 and 13 focusing on the middle frames.

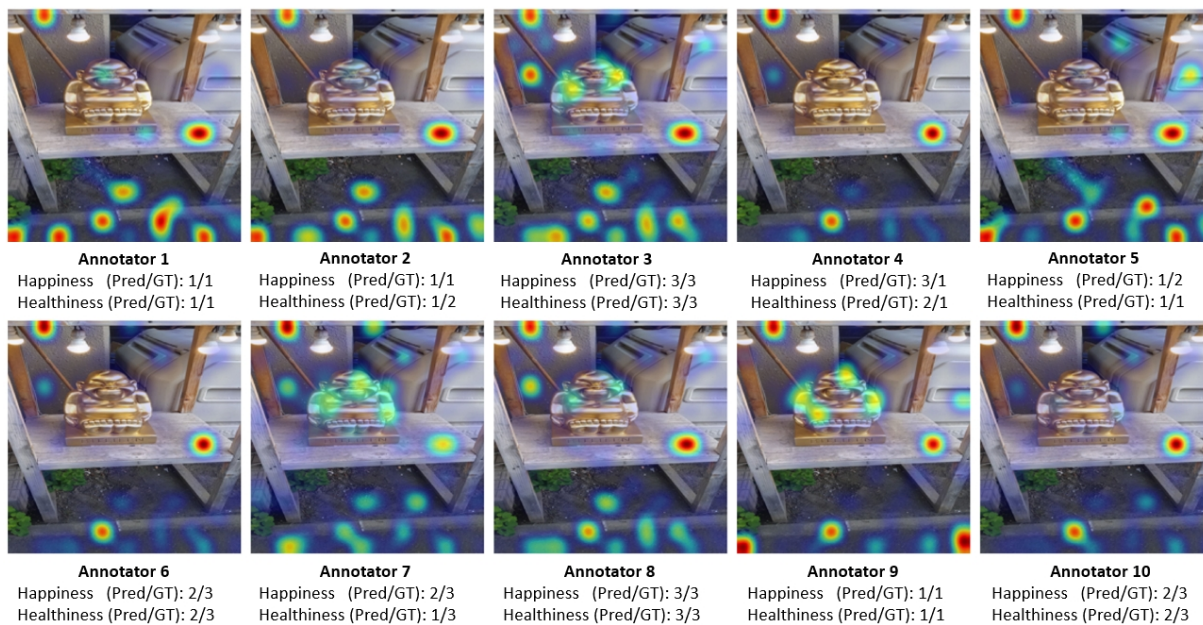


Figure 4: We visualize the interpretable annotator tendencies on the STREET dataset. The attention patterns of 10 annotators reveal distinct preferences, where annotators 3, and 7 exhibit centralized attention to the statue compared to other annotators.

Table 2: For individual annotator modeling performance, we use the Accuracy metric to evaluate our method and baselines on the AMER dataset for each annotator A_k , $k = 1, \dots, 13$, and report the average performance (Avg). Higher is better.

| Methods | A_1 | A_2 | A_3 | A_4 | A_5 | A_6 | A_7 | A_8 | A_9 | A_{10} | A_{11} | A_{12} | A_{13} | Avg |
|-------------|-------------|-------------|-------------|-------------|-------------|-------------|-------------|-------------|-------------|-------------|-------------|-------------|-------------|-------------|
| Base | 0.30 | 0.29 | 0.43 | 0.25 | 0.24 | 0.20 | 0.26 | 0.19 | 0.34 | 0.10 | 0.41 | 0.48 | 0.19 | 0.28 |
| D-LEMA [21] | 0.86 | 0.88 | 0.85 | 0.87 | 0.89 | 0.86 | 0.88 | 0.87 | 0.85 | 0.86 | 0.45 | 0.51 | 0.33 | 0.84 |
| PADL [19] | 0.89 | 0.90 | 0.88 | 0.93 | 0.87 | 0.91 | 0.86 | 0.94 | 0.89 | 0.88 | 0.47 | 0.54 | 0.35 | 0.87 |
| MaDL [11] | 0.93 | 0.91 | 0.90 | 0.89 | 0.90 | 0.88 | 0.90 | 0.89 | 0.87 | 0.97 | 0.50 | 0.53 | 0.37 | 0.88 |
| Ours | 0.94 | 0.93 | 0.93 | 0.94 | 0.94 | 0.92 | 0.93 | 0.95 | 0.93 | 0.93 | 0.59 | 0.61 | 0.40 | 0.92 |

Table 3: For individual annotator modeling performance, we use the Accuracy metric to evaluate our method and baselines on the STREET dataset for each annotator A^k , $k = 1, \dots, 10$, and report the average performance (Avg). Higher is better.

| Perspectives | Methods | A_1 | A_2 | A_3 | A_4 | A_5 | A_6 | A_7 | A_8 | A_9 | A_{10} | Avg |
|--------------|-------------|-------------|-------------|-------------|-------------|-------------|-------------|-------------|-------------|-------------|-------------|-------------|
| Happiness | Base | 0.80 | 0.12 | 0.27 | 0.38 | 0.56 | 0.35 | 0.44 | 0.44 | 0.31 | 0.55 | 0.42 |
| | D-LEMA [21] | 0.85 | 0.71 | 0.44 | 0.36 | 0.70 | 0.43 | 0.46 | 0.54 | 0.41 | 0.47 | 0.54 |
| | PADL [19] | 0.93 | 0.74 | 0.48 | 0.53 | 0.57 | 0.47 | 0.42 | 0.51 | 0.50 | 0.60 | 0.58 |
| | MaDL [11] | 0.91 | 0.77 | 0.44 | 0.38 | 0.70 | 0.47 | 0.46 | 0.54 | 0.48 | 0.47 | 0.56 |
| | Ours | 0.94 | 0.80 | 0.54 | 0.55 | 0.69 | 0.51 | 0.53 | 0.54 | 0.52 | 0.64 | 0.63 |
| Healthiness | Base | 0.77 | 0.19 | 0.14 | 0.47 | 0.87 | 0.36 | 0.43 | 0.44 | 0.51 | 0.54 | 0.47 |
| | D-LEMA [21] | 0.83 | 0.77 | 0.44 | 0.43 | 0.87 | 0.41 | 0.44 | 0.46 | 0.55 | 0.46 | 0.57 |
| | PADL [19] | 0.92 | 0.72 | 0.55 | 0.44 | 0.84 | 0.47 | 0.46 | 0.44 | 0.52 | 0.55 | 0.59 |
| | MaDL [11] | 0.89 | 0.77 | 0.44 | 0.44 | 0.90 | 0.41 | 0.44 | 0.46 | 0.55 | 0.46 | 0.58 |
| | Ours | 0.92 | 0.75 | 0.56 | 0.52 | 0.90 | 0.49 | 0.48 | 0.54 | 0.64 | 0.61 | 0.64 |
| Safety | Base | 0.58 | 0.65 | 0.36 | 0.36 | 0.61 | 0.37 | 0.56 | 0.40 | 0.32 | 0.53 | 0.47 |
| | D-LEMA [21] | 0.62 | 0.69 | 0.27 | 0.41 | 0.50 | 0.46 | 0.48 | 0.40 | 0.35 | 0.50 | 0.47 |
| | PADL [19] | 0.72 | 0.78 | 0.24 | 0.44 | 0.69 | 0.44 | 0.53 | 0.42 | 0.46 | 0.48 | 0.52 |
| | MaDL [11] | 0.63 | 0.63 | 0.27 | 0.32 | 0.61 | 0.38 | 0.46 | 0.42 | 0.36 | 0.52 | 0.46 |
| | Ours | 0.72 | 0.80 | 0.38 | 0.48 | 0.71 | 0.54 | 0.53 | 0.50 | 0.52 | 0.58 | 0.58 |
| Liveliness | Base | 0.79 | 0.60 | 0.53 | 0.46 | 0.76 | 0.30 | 0.35 | 0.36 | 0.53 | 0.57 | 0.53 |
| | D-LEMA [21] | 0.79 | 0.58 | 0.37 | 0.42 | 0.74 | 0.38 | 0.44 | 0.41 | 0.50 | 0.46 | 0.51 |
| | PADL [19] | 0.85 | 0.66 | 0.56 | 0.46 | 0.75 | 0.44 | 0.43 | 0.47 | 0.56 | 0.57 | 0.58 |
| | MaDL [11] | 0.78 | 0.56 | 0.35 | 0.40 | 0.76 | 0.34 | 0.48 | 0.42 | 0.47 | 0.47 | 0.50 |
| | Ours | 0.87 | 0.68 | 0.57 | 0.53 | 0.80 | 0.49 | 0.48 | 0.51 | 0.62 | 0.61 | 0.62 |
| Orderliness | Base | 0.50 | 0.64 | 0.39 | 0.45 | 0.86 | 0.31 | 0.39 | 0.34 | 0.31 | 0.49 | 0.47 |
| | D-LEMA [21] | 0.55 | 0.60 | 0.32 | 0.36 | 0.82 | 0.39 | 0.42 | 0.36 | 0.37 | 0.47 | 0.47 |
| | PADL [19] | 0.73 | 0.65 | 0.44 | 0.45 | 0.93 | 0.45 | 0.45 | 0.36 | 0.42 | 0.63 | 0.55 |
| | MaDL [11] | 0.61 | 0.60 | 0.34 | 0.36 | 0.86 | 0.37 | 0.47 | 0.36 | 0.37 | 0.49 | 0.48 |
| | Ours | 0.74 | 0.71 | 0.52 | 0.55 | 0.94 | 0.47 | 0.54 | 0.44 | 0.56 | 0.62 | 0.61 |

serene emotions associated with the sculpture. The semantic information highlighted by our model’s learned annotator tendencies largely corresponds with expected preferences, further validating our model’s effectiveness in interpreting multi-annotator tendencies.

5.5 Ablation Study

We conducted an ablation study to evaluate the key novel modules, i.e., the query-based annotator modeling and multiple annotator-specific classifiers. In the former, we remove Q-Former to the Base model; in the latter, we only use a unified classifier (w/ U-cl). As shown in Table 5, either of these decreases the overall performance,

highlighting their effectiveness and reasonability in the architecture.

In addition, we also compared the majority voting consensus label training results (Pre-mv) with the majority voting results after modeling individual annotators (Post-mv). Detail setting refers to supplementary material. As shown in Table 5, the performance after individual annotator modeling significantly outperforms the end-to-end majority voting training results on the AMER dataset. Combined with Table 2, which shows high accuracy for the first 10 annotators and low accuracy for the last 3 annotators, we attribute this improvement to the dataset’s distinct subjective patterns between majority and minority groups. This validates our hypothesis

Table 4: DIC scores to evaluate inter-annotator tendency discrepancy patterns on STREET and AMER datasets, lower values indicate better tendency preservation. -Ha, -He, -Sa, -Li, and -Or represents five perspectives of STREET dataset: happiness, healthiness, safety, liveliness, and orderliness.

| Datasets | D-LEMA | PADL | MaDL | Ours |
|----------|--------|------|------|-------------|
| S-Ha | 0.62 | 0.48 | 0.45 | 0.43 |
| S-He | 0.59 | 0.52 | 0.45 | 0.38 |
| S-Sa | 0.36 | 0.32 | 0.29 | 0.24 |
| S-Li | 0.51 | 0.43 | 0.39 | 0.27 |
| S-Or | 0.61 | 0.57 | 0.59 | 0.54 |
| AMER | 0.42 | 0.36 | 0.31 | 0.23 |

Table 5: Ablation study. The average performance of replacing some modules is compared in individual annotator modeling, as well as a performance comparison of label aggregation with and without individual annotator modeling. All are evaluated by accuracy.

| Method | S-Ha | S-He | S-Sa | S-Li | S-Or | AMER |
|----------|------|------|------|------|------|------|
| Base | 0.42 | 0.47 | 0.47 | 0.53 | 0.47 | 0.28 |
| w/ U-cls | 0.50 | 0.56 | 0.49 | 0.56 | 0.49 | 0.69 |
| Pre-mv | 0.62 | 0.62 | 0.56 | 0.58 | 0.60 | 0.43 |
| Post-mv | 0.62 | 0.58 | 0.61 | 0.59 | 0.62 | 0.60 |
| Average | 0.63 | 0.64 | 0.58 | 0.62 | 0.61 | 0.92 |

that the model effectively learns individual tendencies, providing additional information to enhance label aggregation performance. In contrast, the STREET dataset shows less pronounced improvements. Analysis of Table 3 suggests that the modeled annotator tendencies in this dataset are more dispersed, affecting the consensus label aggregation results.

6 CONCLUSION

This paper proposes an explainable framework QuEMAT and constructs two datasets, AMER and STREET. Compared to existing methods, our approach better models the label distribution of each annotator by leveraging both individual annotator modeling and inter-annotator correlations. Additionally, we provide interpretive clues to reveal the behavior of each annotator. The extensive experiments verified the effectiveness of our approach compared with existing methods. After research, we found that through modeling the behavior patterns of individual annotators, we can gain more information about the annotator’s tendency, thereby helping to better implement specific tasks.

Limitations. Multi-annotator tendency learning needs sufficient samples from a single annotator. This is not always the case, especially when crowd-workers are employed for annotation. The required number of annotations by a single annotator is to be explored.

REFERENCES

- [1] Ahmed Almazroa, Sami Alodhayb, Essameldin Osman, Eslam Ramadan, Mohammed Hummadi, Mohammed Dlain, Muhannad Alkatee, Kaamran Raahemifar, and Vasudevan Lakshminarayanan. 2017. Agreement among ophthalmologists in marking the optic disc and optic cup in fundus images. *International ophthalmology* 37 (2017), 701–717.
- [2] Samuel G Armato III, Geoffrey McLennan, Luc Bidaut, Michael F McNitt-Gray, Charles R Meyer, Anthony P Reeves, Binsheng Zhao, Denise R Aberle, Claudia I Henschke, Eric A Hoffman, et al. 2011. The lung image database consortium (LIDC) and image database resource initiative (IDRI): a completed reference database of lung nodules on CT scans. *Medical physics* 38, 2 (2011), 915–931.
- [3] Peng Cao, Yilun Xu, Yuqing Kong, and Yizhou Wang. 2019. Max-mig: an information theoretic approach for joint learning from crowds. *arXiv preprint arXiv:1905.13436* (2019).
- [4] Chaofan Chen, Oscar Li, Daniel Tao, Alina Barnett, Cynthia Rudin, and Jonathan K Su. 2019. This looks like that: deep learning for interpretable image recognition. *Advances in neural information processing systems* 32 (2019).
- [5] Junfan Chen, Richong Zhang, Jie Xu, Chunming Hu, and Yongyi Mao. 2023. A Neural Expectation-Maximization Framework for Noisy Multi-Label Text Classification. *IEEE Transactions on Knowledge and Data Engineering* 35, 11 (2023), 10992–11003. <https://doi.org/10.1109/TKDE.2022.3223067>
- [6] Yuan-Chia Cheng, Zu-Yun Shiau, Fu-En Yang, and Yu-Chiang Frank Wang. 2023. TAX: Tendency-and-Assignment Explainer for Semantic Segmentation with Multi-Annotators. *arXiv preprint arXiv:2302.09561* (2023).
- [7] Wenliang Dai, Junnan Li, Dongxu Li, Anthony Tiong, Junqi Zhao, Weisheng Wang, Boyang Li, Pascale Fung, and Steven Hoi. 2023. InstructBLIP: Towards General-purpose Vision-Language Models with Instruction Tuning. In *Thirty-seventh Conference on Neural Information Processing Systems*. <https://openreview.net/forum?id=vvoWPYqZJA>
- [8] Alexander Philip Dawid and Allan M Skene. 1979. Maximum likelihood estimation of observer error-rates using the EM algorithm. *Journal of the Royal Statistical Society: Series C (Applied Statistics)* 28, 1 (1979), 20–28.
- [9] Melody Guan, Varun Gulshan, Andrew Dai, and Geoffrey Hinton. 2018. Who said what: Modeling individual labelers improves classification. In *Proceedings of the AAAI conference on artificial intelligence*, Vol. 32.
- [10] Asma Ahmed Hashmi, Aigerim Zhumabayeva, Nikita Kotelevskii, Artem Agafonov, Mohammad Yaqub, Maxim Panov, and Martin Takáč. 2023. Learning Confident Classifiers in the Presence of Label Noise. *arXiv preprint arXiv:2301.00524* (2023).
- [11] Marek Herde, Denis Huseljic, and Bernhard Sick. 2023. Multi-annotator Deep Learning: A Probabilistic Framework for Classification. *arXiv preprint arXiv:2304.02539* (2023).
- [12] Wei Ji, Shuang Yu, Junde Wu, Kai Ma, Cheng Bian, Qi Bi, Jingjing Li, Hanruo Liu, Li Cheng, and Yefeng Zheng. 2021. Learning Calibrated Medical Image Segmentation via Multi-rater Agreement Modeling. In *2021 IEEE/CVF Conference on Computer Vision and Pattern Recognition (CVPR)*. 12336–12346. <https://doi.org/10.1109/CVPR46437.2021.01216>
- [13] Wei Ji, Shuang Yu, Junde Wu, Kai Ma, Cheng Bian, Qi Bi, Jingjing Li, Hanruo Liu, Li Cheng, and Yefeng Zheng. 2021. Learning calibrated medical image segmentation via multi-rater agreement modeling. In *Proceedings of the IEEE/CVF Conference on Computer Vision and Pattern Recognition*. 12341–12351.
- [14] Uthman Jinadu, Jesse Annan, Shanshan Wen, and Yi Ding. 2023. Loss Modeling for Multi-Annotator Datasets. *arXiv preprint arXiv:2311.00619* (2023).
- [15] Alex Krizhevsky. 2009. Learning Multiple Layers of Features from Tiny Images. (Jan 2009).
- [16] Junnan Li, Dongxu Li, Silvio Savarese, and Steven Hoi. 2023. Blip-2: Bootstrapping language-image pre-training with frozen image encoders and large language models. In *International conference on machine learning*. PMLR, 19730–19742.
- [17] Zheng Lian, Haiyang Sun, Licai Sun, Kang Chen, Mngyu Xu, Xexin Wang, Ke Xu, Yu He, Ying Li, Jinming Zhao, et al. 2023. Mer 2023: Multi-label learning, modality robustness, and semi-supervised learning. In *Proceedings of the 31st ACM International Conference on Multimedia*. 9610–9614.
- [18] Zheng Lian, Haiyang Sun, Licai Sun, Zhuofan Wen, Siyuan Zhang, Shun Chen, Hao Gu, Jinming Zhao, Ziyang Ma, Xie Chen, et al. 2024. MER 2024: Semi-Supervised Learning, Noise Robustness, and Open-Vocabulary Multimodal Emotion Recognition. In *MRAC’24: Proceedings of the 2nd International Workshop on Multimodal and Responsible Affective Computing*. 41–48.
- [19] Zehui Liao, Shishuai Hu, Yutong Xie, and Yong Xia. 2024. Modeling annotator preference and stochastic annotation error for medical image segmentation. *Medical Image Analysis* 92 (2024), 103028.
- [20] Bjoern Menze, Leo Joskowicz, Spyridon Bakas, Andras Jakab, Ender Konukoglu, Anton Becker, and et al. 2020. Quantification of uncertainties in biomedical image quantification challenge. <https://qubiq.grand-challenge.org/>.
- [21] Zahra Mirikharaji, Kumar Abhishek, Saed Izadi, and Ghassan Hamarneh. 2021. D-lema: Deep learning ensembles from multiple annotations-application to skin lesion segmentation. In *Proceedings of the IEEE/CVF Conference on Computer Vision and Pattern Recognition*. 1837–1846.

- [22] Jeppe Nørregaard and Leon Derczynski. 2022. Sparse Probability of Agreement. *arXiv preprint arXiv:2208.06161* (2022).
- [23] Joshua Peterson, Ruairidh Battleday, Thomas Griffiths, and Olga Russakovsky. 2019. Human uncertainty makes classification more robust. In *2019 IEEE/CVF International Conference on Computer Vision (ICCV)*. <https://doi.org/10.1109/iccv.2019.00971>
- [24] Joshua C Peterson, Ruairidh M Battleday, Thomas L Griffiths, and Olga Russakovsky. 2019. Human uncertainty makes classification more robust. In *Proceedings of the IEEE/CVF international conference on computer vision*. 9617–9626.
- [25] Pranav Rajpurkar, Jeremy Irvin, Aarti Bagul, Daisy Ding, Tony Duan, Hershel Mehta, Brandon Yang, Kaylie Zhu, Dillon Laird, Robyn L Ball, et al. 2017. Mura: Large dataset for abnormality detection in musculoskeletal radiographs. *arXiv preprint arXiv:1712.06957* (2017).
- [26] Vikas C. Raykar, Shipeng Yu, Linda H. Zhao, Gerardo Hermosillo Valadez, Charles Florin, Luca Bogoni, and Linda Moy. 2010. Learning From Crowds. *Journal of Machine Learning Research* 11, 43 (2010), 1297–1322. <http://jmlr.org/papers/v11/raykar10a.html>
- [27] Filipe Rodrigues and Francisco Pereira. 2018. Deep learning from crowds. In *Proceedings of the AAAI conference on artificial intelligence*, Vol. 32.
- [28] Filipe Rodrigues, Francisco Pereira, and Bernardete Ribeiro. 2013. Learning from multiple annotators: distinguishing good from random labelers. *Pattern Recognition Letters* 34, 12 (2013), 1428–1436.
- [29] Filipe Rodrigues, Francisco Pereira, and Bernardete Ribeiro. 2013. Learning from multiple annotators: distinguishing good from random labelers. *Pattern Recognition Letters* 34, 12 (2013), 1428–1436.
- [30] Filipe Rodrigues, Francisco Pereira, and Bernardete Ribeiro. 2014. Gaussian Process Classification and Active Learning with Multiple Annotators. In *Proceedings of the 31st International Conference on Machine Learning (Proceedings of Machine Learning Research, Vol. 32)*, Eric P. Xing and Tony Jebara (Eds.). PMLR, Beijing, China, 433–441. <https://proceedings.mlr.press/v32/rodrigues14.html>
- [31] Mike Schaeckermann, Graeme Beaton, Minahz Habib, Andrew Lim, Kate Larson, and Edith Law. 2019. Understanding Expert Disagreement in Medical Data Analysis through Structured Adjudication. *Proc. ACM Hum.-Comput. Interact.* 3, CSCW, Article 76 (Nov. 2019), 23 pages. <https://doi.org/10.1145/3359178>
- [32] Rion Snow, Brendan O’Connor, Daniel Jurafsky, and Andrew Ng. 2008. Cheap and Fast – But is it Good? Evaluating Non-Expert Annotations for Natural Language Tasks. In *Proceedings of the 2008 Conference on Empirical Methods in Natural Language Processing*, Mirella Lapata and Hwee Tou Ng (Eds.). Association for Computational Linguistics, Honolulu, Hawaii, 254–263. <https://aclanthology.org/D08-1027>
- [33] Quan Sun, Yuxin Fang, Ledell Wu, Xinlong Wang, and Yue Cao. 2023. Eva-clip: Improved training techniques for clip at scale. *arXiv preprint arXiv:2303.15389* (2023).
- [34] Ryutaro Tanno, Ardavan Saeedi, Swami Sankaranarayanan, Daniel C Alexander, and Nathan Silberman. 2019. Learning from noisy labels by regularized estimation of annotator confusion. In *Proceedings of the IEEE/CVF conference on computer vision and pattern recognition*. 11244–11253.
- [35] Ryutaro Tanno, Ardavan Saeedi, Swami Sankaranarayanan, Daniel C. Alexander, and Nathan Silberman. 2019. Learning From Noisy Labels by Regularized Estimation of Annotator Confusion. In *Proceedings of the IEEE/CVF Conference on Computer Vision and Pattern Recognition (CVPR)*.
- [36] Anthony J. Viera and Joanne M. Garrett. 2005. Understanding interobserver agreement: the kappa statistic. *Family Medicine, Family Medicine* (May 2005).
- [37] Chongyang Wang, Yuan Gao, Chenyou Fan, Junjie Hu, Tin Lum Lam, Nicholas D Lane, and Nadia Bianchi-Berthouze. 2023. Learn2agree: Fitting with multiple annotators without objective ground truth. In *International Workshop on Trustworthy Machine Learning for Healthcare*. Springer, 147–162.
- [38] Peter Welinder, Steve Branson, Pietro Perona, and Serge Belongie. 2010. The multidimensional wisdom of crowds. *Advances in neural information processing systems* 23 (2010).
- [39] Jacob Whitehill, Ting-fan Wu, Jacob Bergsma, Javier Movellan, and Paul Ruvolo. 2009. Whose vote should count more: Optimal integration of labels from labelers of unknown expertise. *Advances in neural information processing systems* 22 (2009).
- [40] Yan Yan, Römer Rosales, Glenn Fung, Ramanathan Subramanian, and Jennifer Dy. 2014. Learning from multiple annotators with varying expertise. *Machine learning* 95 (2014), 291–327.
- [41] Hang Zhang, Xin Li, and Lidong Bing. 2023. Video-LLaMA: An Instruction-tuned Audio-Visual Language Model for Video Understanding. In *Proceedings of the 2023 Conference on Empirical Methods in Natural Language Processing: System Demonstrations*. 543–553.
- [42] Le Zhang, Ryutaro Tanno, Moucheng Xu, Yawen Huang, Kevin Bronik, Chen Jin, Joseph Jacob, Yefeng Zheng, Ling Shao, Olga Ciccarelli, et al. 2023. Learning from multiple annotators for medical image segmentation. *Pattern Recognition* 138 (2023), 109400.
- [43] Yifei Zhang, Siyi Gu, Yuyang Gao, Bo Pan, Xiaofeng Yang, and Liang Zhao. 2023. Magi: Multi-annotated explanation-guided learning. In *Proceedings of the IEEE/CVF International Conference on Computer Vision*. 1977–1987.